Natural resources and bioeconomy studies 8/2024

Measuring forest machine rut depth using inexpensive remote sensing methods

A case study in Finland

Henna Kainulainen, Antti Raatevaara, Eero Holmström, Perttu Anttila, Harri Lindeman and Jari Ala-Ilomäki

Luke
LUONNONVARAKESKUS

Natural resources and bioeconomy studies 8/2024

Measuring forest machine rut depth using inexpensive remote sensing methods

A case study in Finland

Henna Kainulainen, Antti Raatevaara, Eero Holmström, Perttu Anttila, Harri Lindeman and Jari Ala-Ilomäki

Natural Resources Institute Finland 2024

Referencing instructions:

Kainulainen, H., Raatevaara, A., Holmström, E., Anttila, P., Lindeman, H. & Ala-Ilomäki, J. 2024. Measuring forest machine rut depth using inexpensive remote sensing methods : A case study in Finland. Natural Resources and Bioeconomy Studies 8/2024. Natural Resources Institute Finland. Helsinki. 21 p.

Eero Holmström's ORCID ID: https://orcid.org/0000-0002-4866-3730

ISBN 978-952-380-874-4 (Online)
ISSN 2342-7639 (Online)
URN urn.fi/URN:ISBN:978-952-380-874-4

Authors: Henna Kainulainen, Antti Raatevaara, Eero Holmström, Perttu Anttila, Harri Lindeman and Jari Ala-Ilomäki
Publisher: Natural Resources Institute Finland (Luke), Helsinki 2024
Year of publication: 2024
Cover picture: Erkki Oksanen, Luke

Abstract

Henna Kainulainen[1], Antti Raatevaara[1, 2], Eero Holmström[1], Perttu Anttila[1], Harri Lindeman[1] and Jari Ala-Ilomäki[1]

[1] Natural Resources Institute Finland, Latokartanonkaari 9, 00790 Helsinki, Finland
[2] MiCROTEC Innovating Wood Oy, Klovinpellontie 1-3, 02180 Espoo, Finland

Forest operations may result in rut formation detrimental to the forest environment. Affordable methods for monitoring rutting are therefore needed. In this study, three inexpensive remote sensing methods were tested for measuring rutting: a drone-based camera using photogrammetry (UAV_{PH}); RGB-depth simultaneous localization and mapping with a mobile stereo camera (RGB-D SLAM); and mobile LiDAR scanning with an iPad (iPad). The measurements were performed at two forest operation sites (A and B) in Finland. Sufficiently reliable results were obtained with UAV_{PH} and RGB-D SLAM on site A, which consisted of open area. Here, UAV_{PH} and RGB-D SLAM produced rut depth estimates with a root-mean-square error (RMSE) of 4 to 7 cm. On site B, trees surrounding the ruts were present. Here, the accuracy of UAV_{PH} was lower than on site A, with an RMSE of 12 and 14 cm for the two ruts respectively. On this site, RGB-D SLAM gave an RMSE as high as 43 and 108 cm due to lower computational power being available during measurement. Pearson's correlation between the remote sensing measurements and reference values was over 0.90 for UAV_{PH} and RGB-D SLAM on site A. On site B, correlation for UAV_{PH} was over 0.70, but correlation for RGB-D SLAM was low. The iPad did not produce results of useful accuracy. With a clear view of the ruts being imaged and with sufficient computational power on site, the UAV_{PH} and RGB-D SLAM methods appear promising approaches for monitoring rut depth in real forest operations, UAV_{PH} being the superior of the two.

Keywords: forest machines, photogrammetry, soil mechanics

Contents

1. Introduction

Rutting is an undesired yet often inevitable part of forest operations. Through water logging, damaged roots, and soil compaction, rutting causes damage to the soil and the environment. Rutting can also have adverse effects on vegetation and tree growth after the operations (Marra et al. 2021a, Pierzchała et al. 2016, Nevalainen et al. 2017, Talbot et al. 2018, Campbell et al. 2013). These negative impacts can take decades to reverse, or they may even be irreversible (Marra et al. 2021a, Haas et al. 2016).

Minimizing rutting and reducing the environmental effects of forest operations is important. Reliable, sufficiently accurate, and preferably inexpensive ways of measuring rutting are needed. Measurements and knowledge of rutting based on past operations can also help in improving the planning of future operations (Marra et al. 2021b, Talbot et al. 2018, Sirén et al. 2013, Campbell et al. 2013). Furthermore, laws and certification standards set criteria for damage caused by harvesting. For example, the Finnish Forest Centre, the body responsible for enforcing forestry legislation in Finland, controls the quality of harvesting through manual field measurements based on sampling. On an inspected site, harvesting is considered erroneous on mineral soils if the share of rut sections of at least 10 cm in depth (20 cm on peatlands) and 1 m in length exceeds 20% (25% on peatlands) of the total rut length (Finnish Forest Centre 2022).

Manual measuring of rut depth is very time-consuming and can in practice only be done on a sparse set of points on the rut network. Clearly, there is a need for more efficient approaches. Photogrammetric methods, both remote and proximal, as well as LiDAR, ultrasound, and cameras, have been researched in measuring rutting due to wheels (Talbot & Astrup 2021, Marra et al. 2021b, Torresan et al. 2017, Talbot et al. 2017, Liang et al. 2015, Haas et al. 2016) and monitoring road conditions (Staniek 2017, Lydon et al. 2020) in recent years. Good results were obtained by Marra et al. (2021b) using UAV-based photogrammetry both in an open field and when the ruts were lined with trees on one side. In Marra et al. (2021b), with UAV-based photogrammetry, and in Pierzchała et al. (2016), with terrestrial close-range photogrammetry using a consumer-grade camera suspended from a pole, it was found that free-standing water in the ruts and vegetation in or near the ruts could cause errors in measurements. This was due to texture issues and the fact that photogrammetry only measures the surfaces of objects. By computing a canopy height model and ground surface models and forming point clouds from UAV-based photogrammetry, reasonable results for rut depth were obtained by Nevalainen et al. (2017), when the ruts were surrounded by forest.

These previously studied approaches have been noted to produce data of unnecessarily high detail and resolution for the task at hand (Talbot & Astrup 2021). For practical purposes in real forest operations, robust and inexpensive methods of low complexity that give reasonably accurate results may be more desirable. The two unexplored methods of terrestrial photogrammetry through stereo imaging and the LiDAR of an iPad tablet, as well as the previously studied drone approach, i.e., UAV-based photogrammetry, are three approaches which might fall into this regime.

This study's objective was to compare these three inexpensive and relatively straightforward remote sensing methods for assessing rut depth on harvesting sites. Specifically, the aim was to evaluate if these methods were sufficiently reliable and accurate to quantify rut depths produced in a real operational setting for monitoring purposes.

2. Materials and methods

2.1. The studied sites

The experiments were conducted in the spring and fall of 2021. Two forest operation sites were studied: site A in Kouvola in South-Eastern Finland, and site B in Rovaniemi in Northern Finland (Fig. 1). The forest operations had been conducted during the previous winter. On site A, all three remote sensing methods, a drone-based camera using photogrammetry (UAV_{PH}), RGB-depth simultaneous localization and mapping with a mobile stereo camera (RGB-D SLAM), and mobile LiDAR scanning with an iPad (iPad), were tested. On site B, only UAV_{PH} and RGB-D SLAM were tested. Manual laser leveler measurements were used as the reference on both sites.

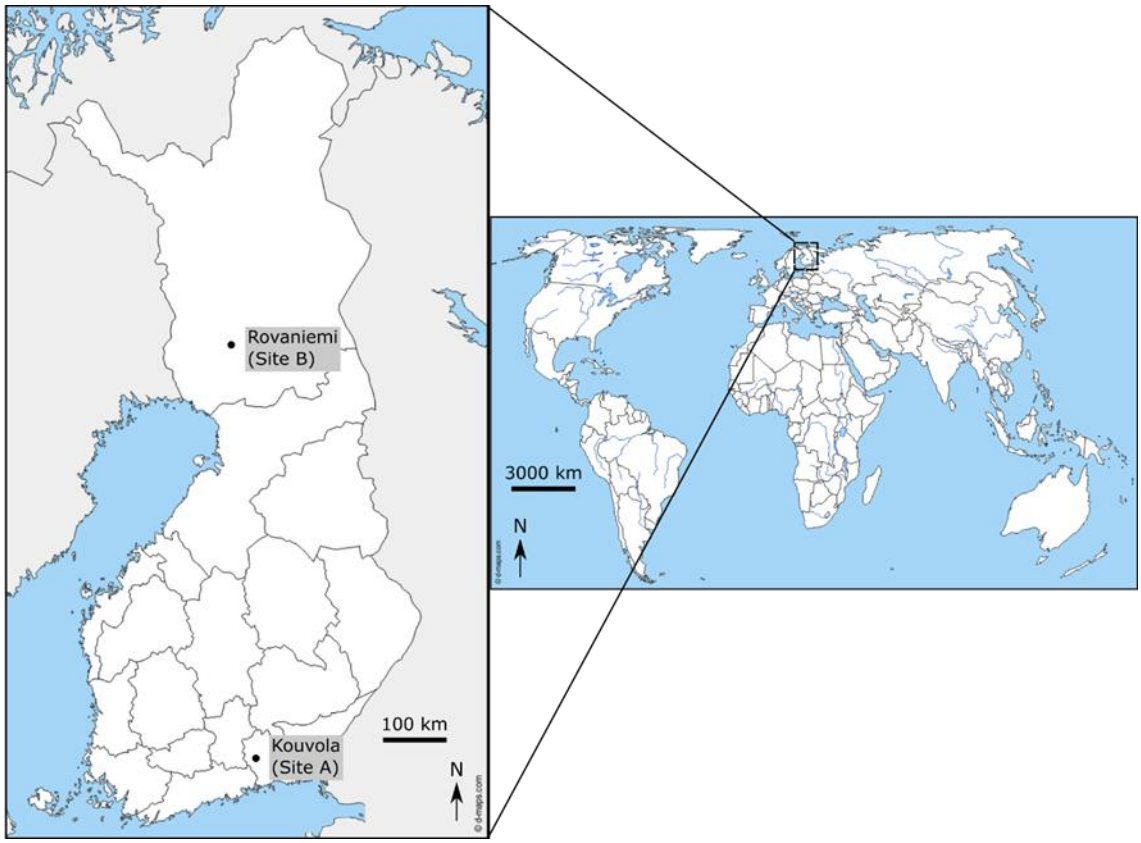

Figure 1. Locations of the two study sites A and B in Finland used in this work. The maps are from https://d-maps.com.

2.2. Remote sensing and ground truth measurements

For UAV_{PH}, the drone and drone camera employed were the Phantom-4 and the DJI FC330 Drone Camera respectively. At site A, the drone was flown at an altitude of approximately 45 m above ground, with a ground sampling distance of 2.5 cm per pixel, a front image overlap of 75%, side overlap of 70%, and a gimbal angle of minus 65 degrees. At site B, the drone was flown at an altitude of approximately 50 m above ground, with a ground sampling distance of 1.5 cm per pixel, a front image overlap of 75%, side overlap of 70%, and a gimbal

angle of minus 65 degrees. The image size was 4000 x 3000 pixels at both sites. The drone imaging was performed in the daytime.

For RGB-D SLAM, the stereo camera used was the Intel RealSense D455, which was attached to a helmet with a custom-made 3D-printed holder for the camera. The RealSense D455 camera is largely a plug-and-play system and thus simple to employ. To perform the RGB-D SLAM measurements, the ruts were traversed from end to end by walking while wearing the helmet with the stereo camera attached. The images were taken at the full resolution of 1280 x 720 pixels. The device calculates depth using stereo vision. It consists first of a pair of RGB cameras, left and right, which are identical and capture light at a wavelength range of 400 to 865 nm. In addition, the device houses an RGB sensor and an infrared projector. The infrared projector projects a non-visible static infrared pattern to improve depth accuracy in low-texture scenes (Intel 2022, Trosin et al. 2021). On site A, an MSI GS65 Thin 8RE laptop was used for the RGB-D SLAM measurements. On site B, an NVIDIA Jetson Nano computer was used instead. The former provided more computational power than the latter. Two different computers were used in order to gauge the sensitivity of the RGB-D SLAM method to real-time computing power.

The iPad used in this study was an iPad Pro 2020. The LiDAR imaging capability of the iPad was used in the measurements (Apple 2020, Apple Insider 2020). Unfortunately, the technical specifications of the LiDAR sensor of the iPad were unavailable.

The ground truth measurements of rut depth were taken along measurement lines perpendicular to the ruts (Table 1, Fig. 2). The positions of the lines along the ruts were chosen aiming at varying rut depth. Altogether, nine lines were measured on site A, and 12 lines on site B. These reference measurements were taken using a laser leveler along each measurement line at every 20 cm, starting on undisturbed ground always to the same side of the ruts within each studied site. The measurement lines were painted on the ground with spray paint to mark them for analysis from the remote sensing materials. There were no logging residues on the ruts, which made the measurement process easier.

On site A, the weather was sunny during the imaging and the manual field measurements on May 24, 2021. Illumination was uneven, and shadows were formed. In addition to a few large trees in the vicinity of the ruts, there was mostly only low vegetation (grass, bushes, and tree saplings). There were several puddles of water along the ruts, but only one measurement line passed through water. Parts of the ruts had shadows directly on them or right at their edges.

On site B, the weather was cloudy, leading to diffuse lighting during the imaging and the manual field measurements on September 16, 2021. The ruts were surrounded by large trees overshadowing the ruts. The ground vegetation consisted mostly of small twigs and heather. There was no water in the ruts on this site.

Table 1. Results for the mean of the absolute value of the laser-leveler, i.e., reference value of maximum rut depth for each remote sensing method, rut, and site. The reference value varies slightly by remote sensing method due to the alignment of the reference and the remote sensing profile (see text). All units are in cm.

remote-sensing method and rut	site A	site B
UAV_{PH}, rut 1	17.8	19.2
UAV_{PH}, rut 2	19.1	26.5
RGB-D SLAM, rut 1	16.0	17.9
RGB-D SLAM, rut 2	19.1	25.1
iPad, rut 1	16.0	not employed
iPad, rut 2	19.1	not employed

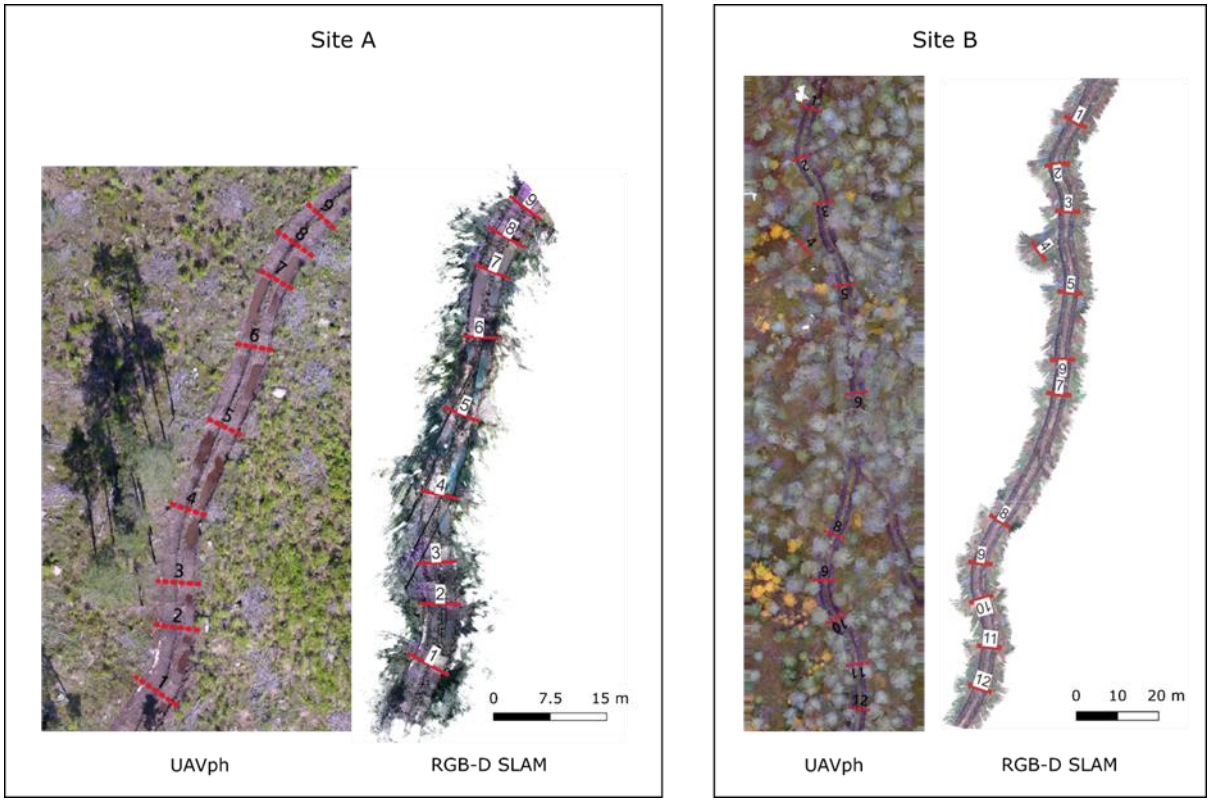

Figure 2. Images of the ruts obtained using UAV_{PH} and RGB-D SLAM on the study sites. The measurement lines have been drawn on the images as red lines, and they have been numbered.

2.3. Post-processing the remote sensing data

For UAV_{PH}, point clouds were computed using OpenDroneMap (OpenDroneMap 2021). For RGB-D SLAM, SLAM modeling in RTABMap (Labbé & Michaud 2019) was used to produce the point clouds. Digital surface models (DSMs) were then computed from the point clouds using a statistical outlier removal (SOR) filter of the PCL library (Rusu & Cousins 2011) and forming a raster surface in CloudCompare (CloudCompare 2021). The iPad measurements produced a point cloud that was processed into a DSM using CloudCompare. The density of

the point clouds differed significantly, depending on the remote sensing method: For RGB-D SLAM (stereo camera), there were on average 25 000 to 100 000 points per m^2 in the middle of the forwarding trail, for UAV_{PH} (drone) on average 5 000 to 7 000 points per m^2, and for iPad, on average 360 000 points per m^2.

Based on the spray paint visible in the images (Fig. 2), the measurement lines were drawn manually on the DSMs. As was the case for the reference measurements, elevation values at every 20 cm along the measurement lines were taken from the DSMs. From these, the rut profiles and rut depth were calculated using the open-source geographical information system QGIS (QGIS 2022) and Python. The SciPy implementation of the Savitzky-Golay filter (Virtanen et al. 2020) was applied to each rut profile, including the reference profile, in order to smooth the data prior to any analysis. For UAV_{PH} on site B, one of the measurement lines was occluded by treetops and could therefore not be imaged. An example of a rut profile and the computed rut depths is given in Fig. 3.

For each line (remote sensing or laser leveler), the first point outside the wheel rut was designated as the level of the undisturbed ground at that line, i.e., elevation of 0 cm, with negative values of elevation lying below it, and positive values above. A different approach was also tested, in which the average elevation of the first three points of a line was computed and then treated as the level of undisturbed ground. This did not have a significant effect on the results of the analysis that followed, so the former approach was used for simplicity.

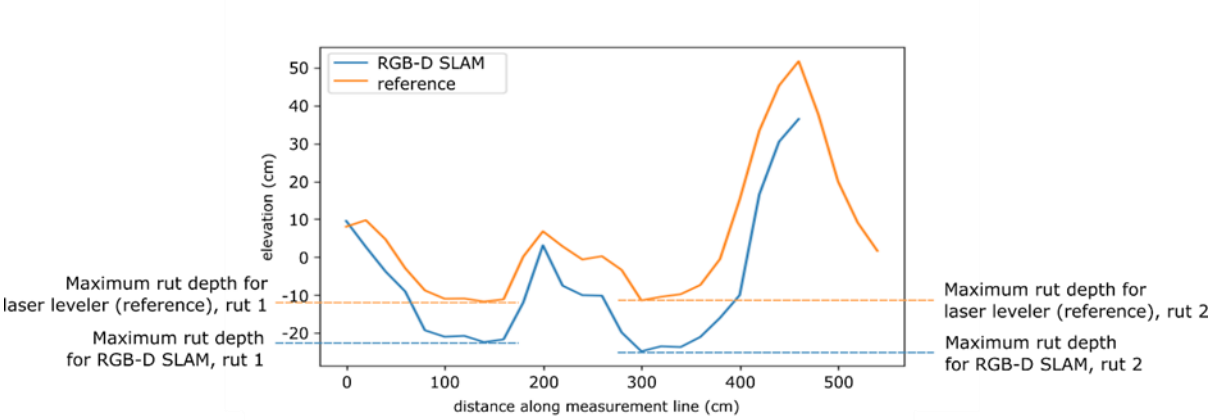

Figure 3. Illustration of an example rut profile from remote sensing (RGB-D SLAM) along a single measurement line, the corresponding laser-leveler reference measurement, and the rut depth measures used in this study. An elevation of 0 cm is the assumed level of undisturbed ground.

2.4. Computing the accuracy of the rut profiles determined by remote sensing

To evaluate the accuracy of the remote sensing methods, the drone, stereo camera, and iPad measurements were aligned with the reference measurements. Vertical alignment had already been achieved by designating, for each measurement method, the first point outside of the wheel rut as having an elevation of 0 cm. Horizontal alignment was then done to facilitate a visual comparison of the rut profile obtained via a given remote sensing method to the laser-leveler reference profile. Indeed, the reference measurements did not necessarily start at the same point on the ground or comprise the same number of measurement points as the

remote sensing measurements did. To accomplish the alignment, each UAV_{PH}, RGB-D SLAM, and iPad measurement rut profile was slid horizontally, in steps of 20 cm, along the reference rut profile until the smallest difference in elevation between the remote sensing and reference rut profile was found. This difference was quantified by the sum of squared errors (Equation 1)

$$\sum_{i=1}^{N}(e_i - \hat{e}_i)^2 \qquad (1)$$

where e_i is the elevation of the ith point along the reference line, $\hat{e}_i$ is the elevation of the ith point along the remote sensing measurement line, and N is the number of points along the shorter line. The sum was taken over those points of the reference measurement and the remote sensing method in question having the same lateral coordinate values, and this dictated the step of 20 cm in sliding the remote sensing profile over the reference profile. The same number of points was always considered when finding the minimum of the sum.

The remote sensing measurement line was then fixed to this horizontal position along the reference line, and the two rut profiles were compared to see how well the remote sensing measurements corresponded to the reference. As the intention was to compare only the corresponding points that both lines had, part of the reference profile or the remote sensing profile was typically cut off from the beginning or the end of the measurement line in this alignment process.

As illustrated in Fig. 3, the quantity of interest in this study was the maximum depth of a rut along the measurement line. In the following, for a given rut, let y_i denote the laser leveler result for maximum depth and let $\hat{y}_i$ denote the remote sensing result for the same along measurement line i. For both studied sites and all remote sensing methods, the root mean square error (RMSE) (Equation 2)

$$\sqrt{\frac{1}{N}\sum_{i=1}^{N}(y_i - \hat{y}_i)^2} \qquad (2)$$

bias (Equation 3)

$$\frac{1}{N}\sum_{i=1}^{N}(y_i - \hat{y}_i) \qquad (3)$$

and mean absolute error (MAE) (Equation 4)

$$\frac{1}{N}\sum_{i=1}^{N}\|y_i - \hat{y}_i\| \qquad (4)$$

were computed along the length of each rut, i.e., over all the measurement lines. RMSE measures the accuracy of the predicted values (remote sensing) against the reference (laser leveler) and is more sensitive to outliers than MAE. A positive value for bias would mean that rut depths for the remote sensing measurements were deeper than for the reference, and vice versa for negative values. In addition, Pearson's correlation coefficient was computed to

further assess how well the remote sensing measurements $\{\hat{y}_i\}$ corresponded to the reference measurements $\{y_i\}$. All units were in centimeters.

Finally, to reflect the Finnish national legislation on the allowed depth of ruts formed in forest operations, a classification of the maximum rut depths, as determined via each remote sensing method, into over and under 10 cm, was performed. For a given site and remote sensing method, this was done by pooling the maximum rut depth values over the two ruts, and then classifying each value accordingly. The success or failure of the classification result for each value was determined by comparing it against the corresponding reference measurement.

3. Results

3.1. Site A

The computed metrics for maximum rut depth at site A are presented for all three remote sensing methods in Table 2. Examples of rut profiles for this site are given in Fig. 4. On this site, given that the mean of the absolute reference rut depth was approximately 20 cm (Table 1, Fig. 4), both UAV_{PH} and RGB-D SLAM gave reasonably accurate results, with the MAE and RMSE falling into an interval of 3 to 7 cm over both methods and ruts (Table 2). The RMSE values are only slightly larger than the corresponding MAE values, indicating the absence of strong outliers. For UAV_{PH}, the difference in maximum rut depth between the remote sensing measurement and the reference was mostly less than 3 cm, but there were some cases where the difference grew larger, for example when there was water in the rut. For RGB-D SLAM, the difference in maximum rut depth between the remote sensing measurements and the reference was mostly less than 5 cm. For both methods, the average rut depths were slightly overestimated, as shown by the positive values of bias in Table 2. In contrast to UAV_{PH} and RGB-D SLAM, the LiDAR-based iPad results are poor, with rut depth overestimated on average by nearly 20 cm.

Pearson's correlation coefficients for the remote sensing results compared with the laser leveler reference values of maximum rut depth are given in Table 3. The correlation for UAV_{PH} and RGB-D SLAM is very high (over 0.90), whereas the result for the iPad is much lower. A scatterplot of the measured versus reference data for all three remote sensing methods on this site is presented in Fig. 6.

Classification results for the rut depths determined by the remote sensing methods on site A are given in Table 4. For UAV_{PH} and RGB-D SLAM, the overall classification accuracy over the 18 data points was 100%. Again, the corresponding iPad results are poor, but the obtained classification accuracy is still a moderate 72%. In the reference measurements, 61% of the ruts were over 10 cm deep, and 39% were less than 10 cm deep.

Table 2. Results for maximum rut depth on site A ($N = 9$ for each rut). Positive bias here means that the rut was estimated to be deeper using the remote sensing method in question than was found using the laser leveler reference measurement.

site A	RMSE (cm)	bias (cm)	MAE (cm)
UAV_{PH}, rut 1	4.3	2.0	3.1
UAV_{PH}, rut 2	6.7	2.5	4.2
RGB-D SLAM, rut 1	4.9	3.2	3.7
RGB-D SLAM, rut 2	6.8	3.2	5.3
iPad, rut 1	22.6	18.7	18.7
iPad, rut 2	24.0	17.8	18.5

Table 3. Pearson's correlation coefficient for maximum rut depth compared with the laser leveler reference values for each site and for each remote sensing method.

rut	UAV_{PH}, site A	RGB-D SLAM, site A	iPad, site A	UAV_{PH}, site B	RGB-D SLAM, site B
rut 1	0.98	0.97	0.76	0.74	0.60
rut 2	0.93	0.95	0.53	0.81	0.04

Table 4. Classification results for maximum rut depth as percentages of true positives (TP), true negatives (TN), false positives (FP), and false negatives (FN) for site A ($N = 18$). Here, positive means deeper than 10 cm, and negative less than 10 cm deep.

site A	TP (%)	TN (%)	FP (%)	FN (%)
UAV_{PH}	61	39	0	0
RGB-D SLAM	61	39	0	0
iPad	61	11	28	0

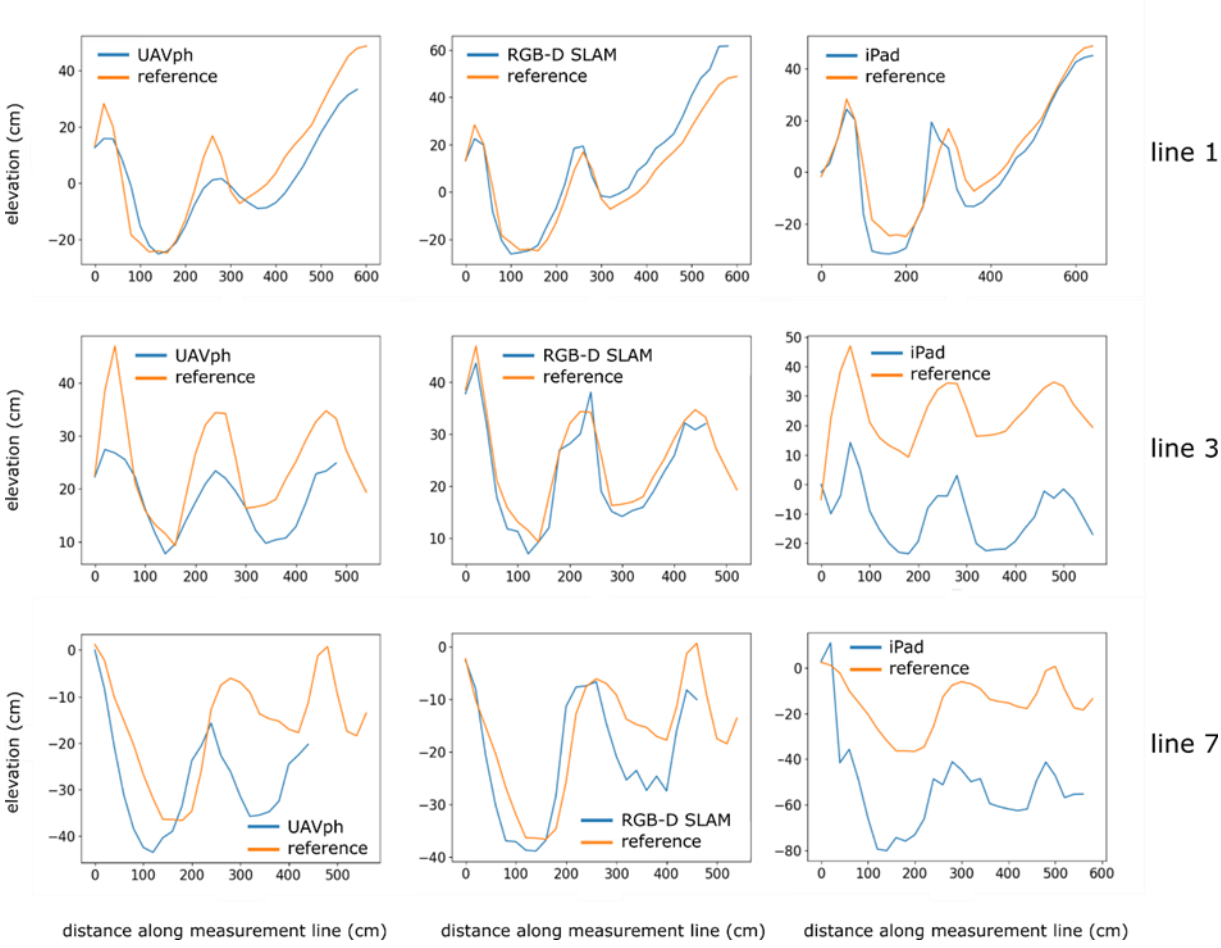

Figure 4. Examples of rut profiles along three different measurement lines on site A using each remote sensing method. These lines were chosen to illustrate the different types of situations found and the results obtained on this site. There was water in the right rut on line 7.

3.2. Site B

The metrics for maximum rut depth on site B are presented for the two remote sensing methods in Table 5. Examples of rut profiles for this site are given in Fig. 5. On this site, given that the mean of the absolute reference rut depth was approximately 20 to 30 cm (Table 1, Fig. 5), UAV_{PH} gave results of fair accuracy, with the MAE and RMSE of rut depth falling between 11 and 14 cm (Table 5). The RMSE values for UAV_{PH} are only slightly larger than MAE values, indicating the absence of clear outliers. However, the RGB-D SLAM approach failed to give results of any useful accuracy on this site. Similar to site A, on average, both methods overestimated rut depth on site B, as shown by the positive values of bias in Table 5.

Pearson's correlation coefficients for the remote sensing results against the laser leveler reference are given in Table 3. The correlation for UAV_{PH} is reasonable (over 0.70), whereas for RGB-D SLAM, the correlation is low. A scatterplot of the measured versus reference data for both remote sensing methods on this site is presented in Fig. 6.

Classification results for the rut depths determined by the two remote sensing methods on site B are given in Table 6. For UAV_{PH}, the overall classification accuracy over the 24 data points was 91%, whereas for RGB-D SLAM the corresponding result was only 67% on this site. In the reference measurements, 67% of the ruts were over 10 cm deep, and 33% were less than 10 cm deep.

Table 5. Results for maximum rut depth on site B ($N = 12$ for each rut). Positive bias here means that the rut was estimated to be deeper using the remote sensing method in question than was found using the laser leveler reference measurement.

site B	RMSE (cm)	bias (cm)	MAE (cm)
UAV_{PH}, rut 1	12.4	2.3	10.7
UAV_{PH}, rut 2	14.0	5.9	12.9
RGB-D SLAM, rut 1	43.3	38.5	38.5
RGB-D SLAM, rut 2	107.7	88.8	88.8

Table 6. Classification results for maximum rut depth as percentages of true positives (TP), true negatives (TN), false positives (FP), and false negatives (FN) for site B ($N = 24$). Here, positive means deeper than 10 cm and negative less than 10 cm deep.

site B	TP (%)	TN (%)	FP (%)	FN (%)
UAV_{PH}	68	23	9	0
RGB-D SLAM	67	0	33	0

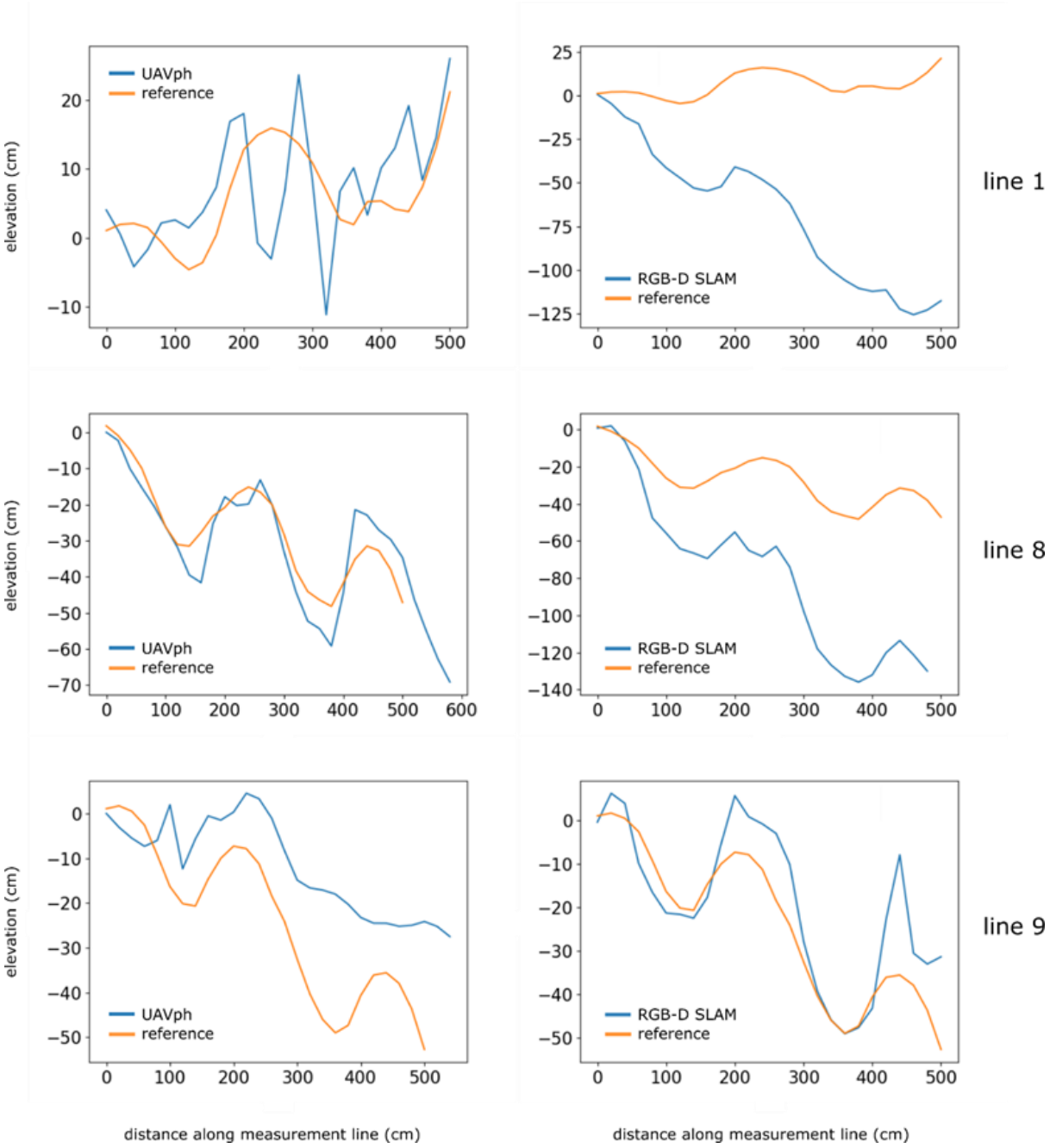

Figure 5. Examples of rut profiles along three different measurement lines on site B using UAV_{PH} and RGB-D SLAM. These lines were chosen to illustrate the different types of situations found and the results obtained on this site.

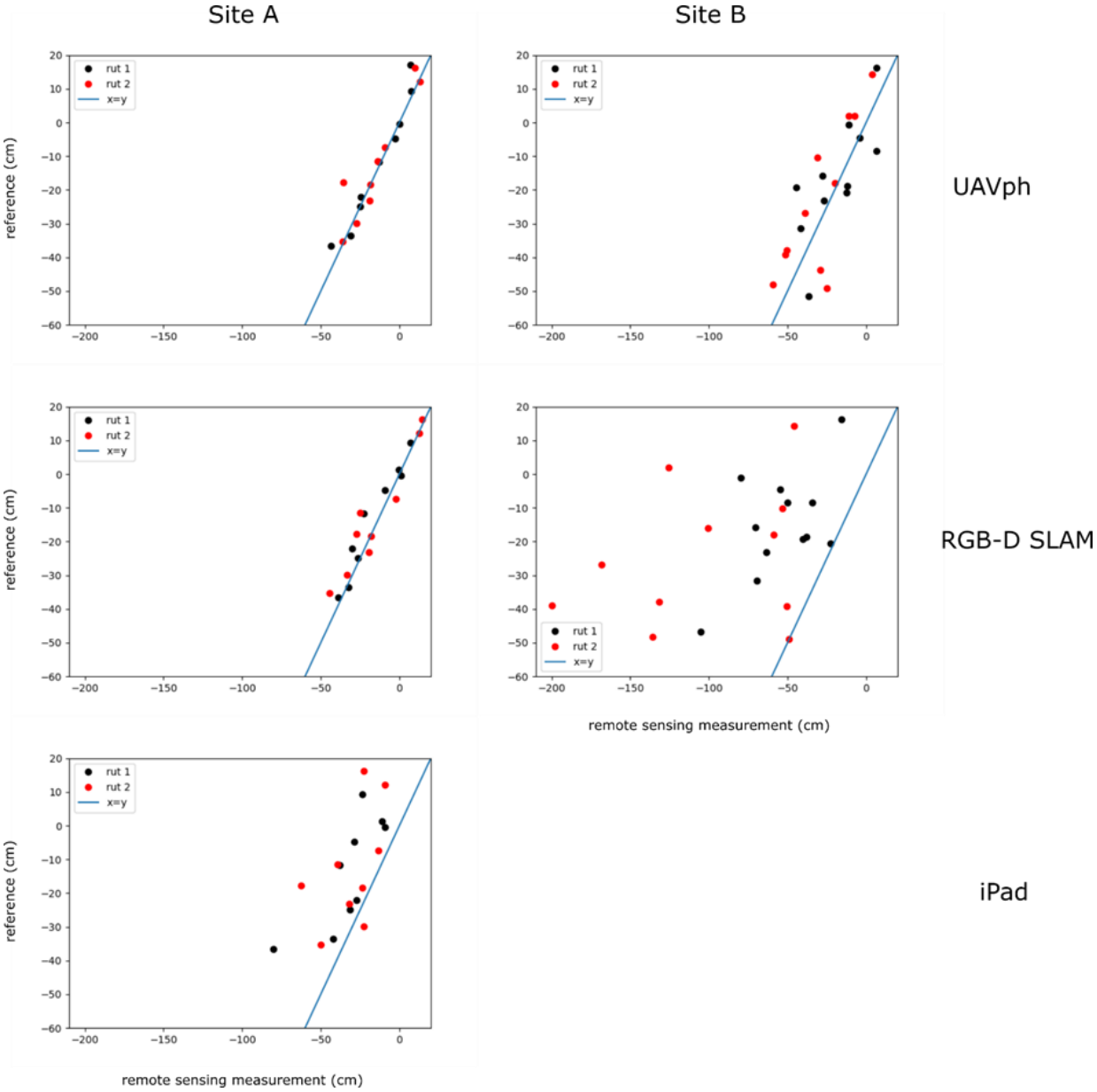

Figure 6. Remote sensing measurements versus reference values for maximum rut depth for each site and each remote sensing method.

4. Discussion

Based on the presented results, it appears that UAV_{PH} produces useful results when employed in good imaging conditions and an open area not occluded by trees, and the method is superior to both the RGB-D SLAM and the iPad approach. When a clear view of the ground is unavailable, less useful information for creating the point clouds is apparently available, resulting in DSMs of lower fidelity. This is deduced from the increase in error from a few cm to approximately 10 cm when moving from site A (Table 2) to site B (Table 5). In contrast, the RGB-D SLAM approach could be expected to work similarly well, regardless of the presence of surrounding trees. The drop from high to low accuracy seen with this method when moving from site A to site B is probably due to less computational power being available for the measurement on site B. Employing the NVIDIA Jetson Nano instead of the laptop computer on site B limited the number of frames that could be collected per second. No such limitation was present when using the MSI GS65 Thin 8RE laptop for the RGB-D SLAM on site A. These findings, as well as the poor performance of the iPad approach in this task, are concisely reflected in the scatterplots of the data presented in Fig. 6.

Results obtained in this study for the RMSE of maximum rut depth as measured by UAV_{PH} on site A, 4.3 cm and 6.7 cm, are similar to the results of Marra et al. (2021b), where the authors found an RMSE of 4.5 cm for rut depth as measured by UAV photogrammetry from the same altitude of 60 m at an open area. Pierzchała et al. (2016) used terrestrial close-range photogrammetry and found an RMSE of 2.1 cm to 3.8 cm between remote sensing and ground truth measurements, as determined for five measurement lines along the entire rut profile for each. This is somewhat more accurate but similar to the RGB-D SLAM result for maximum rut depth on site A in this work, which resulted in an RMSE of 4.9 cm and 6.8 cm for the two ruts, respectively.

The classification results suggest that the UAV_{PH} and RGB-D SLAM methods tend to overestimate rut depth when conditions and computational power are not ideal (Table 6). This tendency is also seen in the positive bias for both methods on both sites (Table 2 and Table 5). For practical applications in monitoring forest operations, the bias found in good conditions and prerequisites, i.e., at site A, is probably sufficiently small to be acceptable by forest operation managers. A positive bias instead of a negative one would probably also be accepted by those in charge of monitoring forest operation quality. Furthermore, provided that the error is indeed systematic, an empirical correction could possibly be derived for the bias.

As regards classifying ruts for monitoring purposes, Nevalainen et al. (2017) found an overall classification accuracy of 65% for rut sections over or under 20 cm in depth using UAV photogrammetry on ruts surrounded by forest. The result of 91% to 100% for classifying maximum rut depth into over or under 10 cm obtained in this work is higher, but the different threshold value for depth, as well as the different and somewhat skewed class distribution here hampers a direct comparison.

The fundamental reason for the poor performance of the iPad approach is unclear. The LiDAR scanner on the device may simply be too weak to perform well in bright sunlight, in which the measurements at site A were produced. It was also found that shadows on or near the ruts had a negative impact on the accuracy of the rut profiles determined with the iPad, but not on the accuracy of the other two remote sensing methods.

All the studied remote sensing methods would be disturbed by water in the ruts, probably for two reasons. First, the measurements cannot probe the ground under the water surface. Second, reflections from the water surface probably hinder the formation of a high-quality photogrammetric point cloud.

To make the UAV_{PH} approach useful in real forest operations, the imaging process should probably be arranged differently. After a thinning operation, flying the drone below the treetops without making contact with trees is probably unattainable with most current commercial solutions, considering, e.g., the decreased GPS accuracy. In clear-cuts, in contrast, measurements would naturally not be hindered by the occlusion of standing trees, and the drone could be made to closely follow the harvesting trail to concentrate the imaging on the area of interest.

Another approach might be to image the site both before and after an operation, produce two ground surface models correspondingly, and then align these at areas of undisturbed ground. One could then estimate the depth of the formed ruts from the difference of the two models. The problem here is that standing trees hinder the creation of an accurate ground model using digital photogrammetry (Graham et al. 2019). Realizing this idea might require using aerial laser scanning instead.

Regarding the RGB-D SLAM approach, attaching a low-cost stereo camera such as RealSense to the rear of the forwarder could be a means to automate the rut depth measurement. Initial tests on another site, not described here in more detail, suggested that attaching the camera to the rear window of a harvester appeared a valid approach. To determine the final depth of ruts produced in an operation, the camera should be installed to, e.g., the rear of the forwarder trailer. Such a solution would require little or no changes to the workflow of the machine operator. High measurement coverage could be achieved with no additional field visits, giving this automated approach of proximal sensing a major advantage over UAV approaches.

Another aspect to consider regarding the applicability of the studied methods to real operations is forest residue on the ruts. In this study, the ruts were free of branches. With moderate amounts of residue, the two photogrammetry-based methods could still be expected to work. However, large amounts of residue would rule these two methods out, while a LiDAR-based approach might still be feasible (Salmivaara et al. 2018).

Finally, the amount of data available for this work was limited. New measurement campaigns are necessary to further scrutinize the usefulness of the presented, inexpensive, and relatively straightforward remote sensing methods in determining rut depth in forest operations. The effect of water on rut depth as measured using these methods should also be studied in detail. It is likely that the studied methods are insufficiently reliable in all practical conditions. However, if favorable conditions could be specified and then observed on the site of an operation, this alone would reduce field work. A further step towards practical applications is the automation of the analysis pipeline for finding rut depth along a set of measurement lines in the remote sensing data. This should be feasible using open-source tools.

5. Conclusions

In this study, three inexpensive relatively straightforward remote sensing approaches were studied to assess whether they could be sufficiently reliable to determine forest machine rut depth for monitoring purposes in real forest operations. It appears that UAV_{PH} (drone-based photogrammetry) and RGB-D SLAM (terrestrial stereo camera) may be feasible approaches, provided that the ruts are not occluded by, e.g., standing trees or logging residues, and that sufficient computational power is available on site. UAV_{PH} performs better of the two. The iPad-based LiDAR approach did not perform well in this task, possibly due to properties of the specific sensor. Although the results are promising, further research is needed to identify the conditions and operational arrangements in which UAV_{PH} and RGB-D SLAM are sufficiently reliable for practical operations.

References

Apple 2020. Apple unveils new iPad Pro with breakthrough LiDAR scanner and brings trackpad support to iPadOS. Available at https://www.apple.com/newsroom/2020/03/apple-unveils-new-ipad-pro-with-lidar-scanner-and-trackpad-support-in-ipados/

Apple Insider 2020. What you need to know about Apple's LiDAR Scanner in the iPad Pro. Available at https://appleinsider.com/articles/20/03/18/what-you-need-to-know-about-apples-lidar-scanner-in-the-ipad-pro

Campbell, D.M.H., White, B. & Arp, P.A. 2013. Modeling and mapping soil resistance to penetration and rutting using LiDAR-derived digital elevation data. Journal of Soil and Water Conservation 68.6: 460–473.

CloudCompare [GPL Software] 2021. Retrieved from https://www.cloudcompare.org/

Finnish Forest Centre 2022. Inspection instructions 2022. [Tarkastusohje 2022]. Available at https://www.metsakeskus.fi/sites/default/files/document/tarkastusohje.pdf. Accessed August 16, 2022.

Graham, A., Coops, N.C., Wilcox, M. & Plowright, A. 2019. Evaluation of ground surface models derived from unmanned aerial systems with digital aerial photogrammetry in a disturbed conifer forest. Remote Sensing 11(1): 84.

Haas, J., Hagge Ellhöft, K., Shack-Kirchner, H. & Lang, F. 2016. Using photogrammetry to assess rutting caused by a forwarder—A comparison of different tires and bogie tracks. Soil and Tillage Research 163: 14–20.

Intel 2022. Intel RealSense Product Family D400 Series datasheet, available at https://www.intelrealsense.com/wp-content/uploads/2022/05/Intel-RealSense-D400-Series-Datasheet-April-2022.pdf. Accessed January 26, 2023.

Labbé, M. & Michaud, F. 2019. RTAB-Map as an open-source lidar and visual simultaneous localization and mapping library for large-scale and long-term online operation. Journal of Field Robotics 36(2): 416–446. Code available at http://introlab.github.io/rtab-map/

Liang, X., Wang, Y., Jaakkola, A., Kukko, A., Kaartinen, H., Hyyppä, J., Honkavaara, E. & Liu, J. 2015. Forest data collection using terrestrial image-based point clouds from a handheld camera compared to terrestrial and personal laser scanning. IEEE transactions on geoscience and remote sensing 53(9): 5117–5132.

Lydon, D., Taylor, S.E., Lydin, M. & Early, J. 2020. A review of vision based methods for pothole detection and road profile analysis. Civil Engineering Research in Ireland 2020. pp. 442–447.

Marra, E., Laschi, A., Fabiano, F., Foderi, C., Neri, F., Mastrolonardo, G., Nordfjell, T. & Marchi, E. 2022. Impacts of wood extraction on soil: assessing rutting and soil compaction caused by skidding and forwarding by means of traditional and innovative methods. European Journal of Forest Research 141(1): 1–16.

Marra, E., Wictorsson, R., Bohlin, J., Marchi, E. & Nordfjell, T. 2021. Remote measuring of the depth of wheel ruts in forest terrain using a drone. International Journal of Forest Engineering 32(3): 224–234.

Nevalainen, P., Salmivaara, A., Ala-Ilomäki, J., Launiainen, S., Hiedanpää, J., Finér, L., Pahikkala, T. & Heikkonen, J. 2017 Estimating the rut depth by UAV photogrammetry. Remote Sensing 9(12): 1279.

OpenDroneMap Authors ODM – A command line toolkit to generate maps, point clouds, 3D models and DEMs from drone, balloon or kite images. OpenDroneMap/ODM GitHub Page 2021; https://github.com/OpenDroneMap/ODM

Pierzchała, M., Talbot, B. & Astrup, R. 2016. Measuring wheel ruts with close-range photogrammetry. Forestry: An International Journal of Forest Research 89(4): 383–391.

QGIS.org 2022. QGIS Geographic Information System. QGIS Association. http://www.qgis.org

Rusu, R.B. & Cousins, S. 2011 3d is here: Point cloud library (pcl). IEEE international conference on robotics and automation. IEEE 2011.

Salmivaara, A., Miettinen, M., Finér, L., Launiainen, S., Korpunen, H., Tuominen, S., Heikkonen, J., Nevalainen, P., Sirén, M., Ala-Ilomäki, J. & Uusitalo, J. 2018. Wheel rut measurements by forest machine-mounted LiDAR sensors–accuracy and potential for operational applications? International Journal of Forest Engineering 29(1): 41–52.

Sirén, M., Ala-Ilomäki, J., Mäkinen, H., Lamminen, S. & Mikkola, T. 2013. Harvesting damage caused by thinning of Norway spruce in unfrozen soil. International Journal of Forest Engineering 24(1): 60–75.

Staniek, M. 2017. Stereo vision method application to road inspection. The Baltic Journal of Road and Bridge Engineering 12(1): 38–47.

Talbot, B., Pierzchałam M. & Astrup, R. 2017. Applications of remote and proximal sensing for improved precision in forest operations. Croatian Journal of Forest Engineering: Journal for Theory and Application of Forestry Engineering 38(2): 327–336.

Talbot, B., Rahlf, J. & Astrup, R. 2018. An operational UAV-based approach for stand-level assessment of soil disturbance after forest harvesting. Scandinavian Journal of Forest Research 33(4): 387–396.

Talbot, B. & Astrup, R. 2021. A review of sensors, sensor-platforms and methods used in 3D modelling of soil displacement after timber harvesting. Croatian Journal of Forest Engineering: Journal for Theory and Application of Forestry Engineering 42(1): 149–164.

Torresan, C., Berton, A., Carotenuto, F., Di Gennaro, S.F., Gioli, B., Matese, A., Miglietta, F., Vagnoli, C., Zaldei, A. & Wallace, L.O. 2017. Forestry applications of UAVs in Europe: A review. International Journal of Remote Sensing 38(8–10): 2427–2447.

Trosin, M., Dekemati, I. & Szabó, I. 2021. Measuring soil surface roughness with the RealSense D435i. Acta Polytechnica Hungarica 18(6): 141–155.

Virtanen, P. et al. 2020. SciPy 1.0: fundamental algorithms for scientific computing in Python. Nature methods 17(3): 261–272.

Luke
LUONNONVARAKESKUS

You can find us online

luke.fi

Natural Resources Institute Finland (Luke), Latokartanonkaari 9, 00790 Helsinki, Finland